Detection of Coupling in Short Physiological Series by a Joint Distribution Entropy Method

Peng Li, *Member, IEEE*, Ke Li, *Member, IEEE*, Chengyu Liu, *Member, IEEE*, Dingchang Zheng, Zong-Ming Li, *Senior Member, IEEE*, and Changchun Liu*

Abstract*—*Objective: **In this study, we developed a joint distribution entropy (JDistEn) method to robustly estimate the coupling in short physiological series.** ***Methods:*** **The JDistEn method is derived from a joint distance matrix which is constructed from a combination of the distance matrix corresponding to each individual data channel using a geometric mean calculation. A coupled Rössler system and a coupled dual-kinetics neural mass model were used to examine how well JDistEn performed, specifically, its sensitivity for detecting weak coupling, its consistency in gauging coupling strength, and its reliability in processing input of decreased data length. Performance of JDistEn in estimating physiological coupling was further examined with bivariate electroencephalography data from rats and RR interval and diastolic time interval series from human beings. Cross-sample entropy (XSampEn), cross-conditional entropy (XCE), and Shannon entropy of diagonal lines in the joint recurrence plots (JENT) were applied for purposes of comparison.** ***Results:*** **Simulation results suggest that JDistEn showed markedly higher sensitivity than XSampEn, XCE, and JENT for dynamics in weak coupling, although as the simulation models were more intensively coupled, JDistEn performance was comparable to the three others. In addition, this improved sensitivity was much more pronounced for short datasets. Experimental results further confirmed that JDistEn outperformed XSampEn, XCE, and JENT for detecting weak coupling, especially for short physiological data.** ***Conclusion:*** **This study suggested that our proposed JDistEn could be useful for continuous and even real-time coupling analysis for physiological signals in clinical practice.**

***Index Terms*—Cardiovascular dynamics, coupling, cross-conditional entropy (XCE), cross-sample entropy (XSampEn), diastolic time interval (DTI), electroencephalography (EEG), joint distribution entropy (JDistEn), joint recurrence plot, neural mass model (NMM), RR interval (RRI).**

I. Introduction

TIME-SERIES analysis methods have been extensively used for understanding neurological control mechanisms in cerebrovascular, cardiovascular, and cardiorespiratory systems. These systems are composed of a myriad of structural units that are highly interconnected, resulting in a degree of coupling which transiently changes over time and under different physiological or pathological states [1]–[6]. Means of reliably estimating such coupling has recently attracted increasing attention.

Due to the nonlinear nature of physiological systems, traditional linear time- and frequency-domain methods, such as crosscorrelation and crosscoherence, although extensively used [7], cannot fully describe the interactions among these highly complex biosystems. Advances in nonlinear dynamics and chaos theory suggest that a number of nonlinear methods are better able to detect the amplitude or phase relations between trajectories in the state space, such as generalized synchronization [8], dynamical interdependence [9], and phase synchronization [2], [10], [11]. However, to achieve reliable estimations, these methods usually require a long time-series (usually over 10 000 or more sampling points) [12], and thus, may not be acceptable in clinical examination with a short screening time or in real-time point-of-care monitoring [13].

A combination of chaos theory and information theory has fostered the development of several methods for describing entropy that show great potential for short-term analysis. These methods include crossapproximate entropy [14], cross-sample entropy (XSampEn) [15], crossconditional entropy (XCE) [16], and Shannon entropy of diagonal lines with different lengths in joint recurrence plots (JENT) [17], among others. Typically, these methods require a predefined threshold parameter [18]–[20] for judging the similarity or "recurrence" of vectors in the state space. Although some "rules of thumb" have been advocated, e.g., using a percent of the maximum state-space diameter or a percent of the standard deviation of the time series [21], it remains a matter of debate to define an appropriate threshold [22]. A tiny variation of the threshold may lead to a considerable change in calculation of similar or recurrent vectors. This instability caused by the threshold parameter may be aggravated in the context of a short dataset. Although these methods were proved acceptable with limited data samples (usually several thousand sampling points or more), less study has been performed to achieve reliable estimations from a short dataset (e.g., 1000 sampling points or less) [16], [23].

It should be noted that the above limitations arise from the kernel algorithms for univariate analysis (e.g., approximate entropy [24], sample entropy [25], conditional entropy [26], and Shannon entropy of diagonal lines in recurrence plots [27]). Solutions for univariate algorithms can therefore be employed to eliminate the limitations in multivariate analysis.

Manuscript received February 23, 2015; revised November 23, 2015; accepted January 2, 2016. Date of publication January 7, 2016; date of current version October 18, 2016. This work was supported by the National Natural Science Foundation of China under Grant 61471223, Shandong Provincial Natural Science Foundation of China under Grant ZR2015FQ016, the China Postdoctoral Science Foundation under Grant 2014M561933, and the Young Scientists Fund of the National Natural Science Foundation of China under Grant 31200744. *Asterisk indicates corresponding author.*

P. Li, K. Li, and Chengyu Liu are with the School of Control Science and Engineering, Shandong University.

*Changchun Liu is with the School of Control Science and Engineering, Shandong University, Jinan 250061, China (e-mail: changchunliu@sdu.edu.cn).

D. Zheng is with the Health & Wellbeing Academy, Faculty of Medical Science, Anglia Ruskin University.

Z.-M. Li is with the Department of Biomedical Engineering, Cleveland Clinic.

This paper has supplemental material available online at http://ieeexplore.ieee.org (File size: 1 MB).

Color versions of one or more of the figures in this paper are available online at http://ieeexplore.ieee.org.

Digital Object Identifier 10.1109/TBME.2016.2515543

Most recently, we have developed a novel distribution entropy (DistEn) method for testing complexity of univariate physiological time series [28]. DistEn is defined from all the intervector distances in the state space; this approach differs from traditional methods, which consider only recurrent vectors. Therefore, DistEn is less affected by data length. A previous study found that DistEn could achieve good reliability even with the data length decreased to only 50 points [28].

In this paper, we show how we came to develop a novel algorithm for quantifying the coupling of bivariate time series based on DistEn. First, a joint distance matrix, derived from the univariate distance matrices corresponding to all data channels through computing the geometric mean, was constructed. The new bivariate algorithm, named joint distribution entropy (JDistEn), was then constructed by combining the joint distance matrix and DistEn. Finally, the performance of the proposed JDistEn was initially examined on a coupled Rössler system and a coupled dual-kinetics neural mass model (NMM), then validated using short-term bivariate rat electroencephalography (EEG) data and coupling data between the human RR interval and diastolic time interval (RRI-DTI) time series.

II. Algorithm for JDistEn

A. Distribution Entropy

By definition, DistEn quantifies the amount of information contained in the state space of time series through estimating the distribution feature of intervector distances. In our last study [28], the amount of information in state space was considered as a certain representation of time-series complexity, as evidenced by the fact that time series with different dynamical regimes have distinctly different distributions. Evaluation of benchmark data demonstrated that a time series with chaotic regime is accompanied by dispersedly distributed intervector distances suggesting large amount of information, whereas the distribution becomes concentrative for periodic time series which are thus characterized by smaller amount of information [28]. In addition, time series with the same dynamical regime (e.g., periodic regime) could indicate different complexity levels since they do not necessarily have the same distribution feature in the state space.

For a time-series $\{u(i), i = 1, 2, \ldots, N\}$, the DistEn algorithm is summarized briefly as follows [28]:

1) State-space reconstruction
   Form $\mathbf{X}(i)$ by $\mathbf{X}(i) = [u(i), u(i+1), \ldots, u(i+m-1)]$, where $i = 1, 2, \ldots, N-m$, m represents the embedding dimension, and $\mathbf{X}(i)$ the vectors in the state space.
2) Distance matrix construction
   Define the intervector distance matrix $\mathbf{D}$ using
   $$\mathbf{D} = \{\|\mathbf{X}(i), \mathbf{X}(j)\|, i, j = 1, 2, \ldots\}, \quad (1)$$
   where $\|\|$ indicates any kind of norm functions. The maximum norm has been applied in the DistEn algorithm.
3) Probability density estimation
   Estimate the empirical probability density function (ePDF) of distance by the histogram of all elements except the main diagonal of $\mathbf{D}$ with B bins. Denote the probability (p) of each bin by p_t, where $t = 1, 2, \ldots, B$.
4) DistEn calculation
   DistEn is calculated from the formula for the Shannon information with a normalization
   $$\mathrm{DistEn}(m, B) = -\frac{1}{\log_2(B)} \sum_{t=1}^{B} p_t \log_2(p_t). \quad (2)$$

B. Joint Distance Matrix

For bivariate series $[u_1(i); u_2(i)]$, $i = 1, 2, \ldots, N$, each data channel is rescaled to fit the range 0 to 1 by

$$\widehat{u}_\varphi(i) = \frac{u_\varphi(i) - \min(u_\varphi)}{\max(u_\varphi) - \min(u_\varphi)} \quad (3)$$

where $\varphi = 1, 2$.

Define the joint distance matrix $\mathbf{JD}$ as

$$\mathbf{JD} = \mathbf{J} - \sqrt{(\mathbf{J} - \mathbf{D}_1)(\mathbf{J} - \mathbf{D}_2)} \quad (4)$$

where $\mathbf{J}$ indicates the all-ones matrix and $\mathbf{D}_\varphi$ the distance matrix of channel φ ($\varphi = 1, 2$). Both the multiplication and the square-root calculations are performed element by element.

C. Joint Distribution Entropy

The JDistEn algorithm is developed by combining the joint distance matrix and DistEn. For the sake of a general definition, different embedding dimensions m_φ are used for the reconstruction of different data channels, and a time delay τ_φ is introduced for each reconstruction process (here, $\varphi = 1, 2$). For the bivariate series $[u_1(i); u_2(i)]$, $i = 1, 2, \cdots, N$, the JDistEn algorithm is introduced as follows.

1) Bivariate state-space reconstruction
   Rescale each data channel using (3), then reconstruct each rescaled $\widehat{u}_\varphi(i)$ to the state space separately with embedding dimension m_φ and time delay τ_φ for each $\varphi = 1, 2$ by
   $$\mathbf{X}_\varphi(i) = \left[\widehat{u}_\varphi(i), \widehat{u}_\varphi(i+\tau_\varphi), \cdots, \widehat{u}_\varphi(i+(m_\varphi-1)\tau_\varphi)\right], \quad (5)$$
   where $i = 1, 2, \cdots, N-n$ and $n = \max(m_\varphi) \times \max(\tau_\varphi)$.
2) Joint distance matrix construction
   Define the distance matrix $\mathbf{D}_\varphi$ for each series separately by
   $$\mathbf{D}_\varphi = \{\|\mathbf{X}_\varphi(i), \mathbf{X}_\varphi(j)\|, i, j = 1, 2, \ldots, N-n\}, \quad (6)$$
   where $\|\|$ indicates the maximum norm. Equation (4) is then used to define the joint distance matrix $\mathbf{JD}$.
3) Probability density estimation
   Estimate the ePDF of distance from the histogram of all elements except the main diagonal of $\mathbf{JD}$, and then, use Doane's formula to determine the optimal number of histogram bins [29]
   $$B = 1 + \log_2(n) + \log_2(1 + |g_1| / \sigma_{g_1}), \quad (7)$$
   where n indicates the total number of observations, g_1 the skewness, and $\sigma_{g_1} = \sqrt{6(n-2)/[(n+1)(n+3)]}$.

4) JDistEn calculation
Define JDistEn by the formula for the Shannon information

$$\mathrm{JDistEn}\,(m,\tau) = -\frac{1}{\log_2(B)}\sum_{t=1}^{B} p_t \log_2(p_t). \quad (8)$$

The normalization by $\log_2(B)$ was to consolidate results from different values of B. The theoretical lower and upper limits of JDistEn should be 0 and 1, corresponding to one-peak and fully flat ePDF. It should be noted that $p_t \log_2(p_t) = 0$ when $p_t = 0$ is followed in both (2) and (8).

III. Evaluation of Simulation Models

A. Evaluation of Coupled Rössler System

1) Model Description: The unidirectional drive-response coupled Rössler system, described as

$$\begin{aligned}
\dot{x}_d &= -\omega_d y_d - z_d \\
\dot{y}_d &= \omega_d x_d + 0.15 y_d \\
\dot{z}_d &= 0.2 + z_d (x_d - 10) \\
\dot{x}_r &= -\omega_r y_r - z_r + k (x_d - x_r) \\
\dot{y}_r &= \omega_r x_r + 0.15 y_r \\
\dot{z}_r &= 0.2 + z_r (x_r - 10)
\end{aligned} \quad (9)$$

was used, wherein the subscripts d and r denote the coordinates for the drive and response systems, respectively, and k the coupling strength. The ω_d and ω_r are forced to be nonidentical by $\omega_{d,r} = 1 \mp \nu$ (identical when $\nu = 0$). Zheng and Hu demonstrated the synchrony of the dynamics with different assignments for ν and k [30]. The equations were integrated using the variable step Runge–Kutta method (the ode45 differential equation solver in MATLAB, MathWorks, Natick, Massachusetts, USA) with an initial step of 0.05, a maximum step of 0.05, and a sampling interval of 0.3. A total of 1500 sampling points were obtained for each variable, but the first 500 points were excluded to ensure that the dynamics had stabilized. Time series of x_d and x_r were taken as observables.

2) Quantification of a Given Method's Sensitivity: Sensitivity is crucial for any coupling method since that factor determines a given method's capacity for detecting weak couplings. Sensitivity is defined by the critical coupling strength at which the distribution $\rho_k^H(x)$ of a specific coupling measure H was significantly different from $\rho_0^H(x)$ [12]. According to Smirnov and Andrzejak's work [12], this can be obtained as follows.

The probability that a random sample from $\rho_k^H(x)$ has a higher value of H than a random sample from $\rho_0^H(x)$ is given by

$$p_H(k) = \int_{-\infty}^{\infty}\left[\int_{-\infty}^{\infty}\rho_0^H(x')\,dx'\right]\rho_k^H(x'')\,dx''. \quad (10)$$

The established XSampEn, XCE, and JENT methods were taken as comparative methods. Their algorithms were described in the Online Supplement. Due to the inverse relationship between XSampEn and k, $\rho_k^H(x)$ and $\rho_0^H(x)$ for XSampEn were switched before inputting to (10). The same process was done for XCE. Thus, by construction, we get $p_H(0) = 0.5$, and values of 1 are obtained if every value from $\rho_k^H(x)$ is greater (or less) than every value from $\rho_0^H(x)$. According to [12], we used a critical value k_{95} at which $p_H(k_{95}) = 0.95$ to quantify and compare the sensitivity of the four methods.

The first coupling was simulated with the identical coupled Rössler dynamics by setting $\nu = 0$ and for the second one by setting $\nu = 0.02$ to have almost identical coupled dynamics. Weak couplings were introduced by varying k from zero to 0.03 in steps of 0.001 for each value of ν. A total of 100 time series were produced to estimate the distributions of the four methods for each combination of ν and k.

For calculations using the four methods, the embedding dimension m and time delay τ were set at 3 and 11, respectively, for both channels according to a differential entropy-based method (see Section III in Online Supplement) [31]. The threshold value r was set at 0.15 for XSampEn, the quantization level at $\xi = 6$ for XCE, and minimum diagonal line length at $l_{\min} = 2$ for JENT.

3) Estimation of Coupling Strength: It is expected that a given coupling method should shift monotonously toward higher (or lower) values with coupling strength k. To evaluate how well each of the four methods estimated coupling, we compared their performance with a full range of k, from uncoupled ($k = 0$) to strongly coupled dynamics ($k = 0.2$) [30] with a stepsize of 0.005. The two examples—identical and almost identical coupled dynamics—were used again by setting $\nu = 0$ and $\nu = 0.02$, respectively. We estimated the values of XSampEn, XCE, JENT, and JDistEn using ensembles of 100 realizations for each combination of ν and k. All input parameters for the calculation followed the same setting in Section III-A-2 of this section.

4) Effect of Data Length: To further understand the performance of the four methods for extremely short datasets, we reperformed the coupling analysis on coupled Rössler systems with $\nu = 0$ and $\nu = 0.02$, as described above. But this time, we truncated the datasets and retained the first 100 sampling points for the analysis.

5) Evaluation Results on the Coupled Rössler Systems:

a) Sensitivity: Fig. 1 shows the sensitivity results from the four methods with $\nu = 0$ and Fig. S2 (see the Online Supplement) with $\nu = 0.02$. The $p_H(k)$ values of XSampEn and JENT did not reach the sensitivity threshold value 0.95 for all tested coupling strengths from zero to 0.03 for both the identical and almost identical coupled Rössler systems. It should be noted that although $p_H(k)$ of XSampEn for $\nu = 0.02$ reached the threshold value 0.95 once at $k = 0.15$ to 0.2, it finally dropped below it, as shown in Fig. S2 (a2). XCE for $\nu = 0$ indicated a critical coupling strength 0.009 as shown in Fig. 1(b2). However, as shown in Fig. S2(b2) for $\nu = 0.02$, it failed to show such a critical k value.

By comparison, JDistEn achieved significantly improved sensitivity for both coupling systems. The critical coupling strength was as low as 0.004 for $\nu = 0$. In addition, although the three other methods failed for $\nu = 0.02$, DistEn still showed a relatively low critical value $k_{95} = 0.01$. Note that in some cases

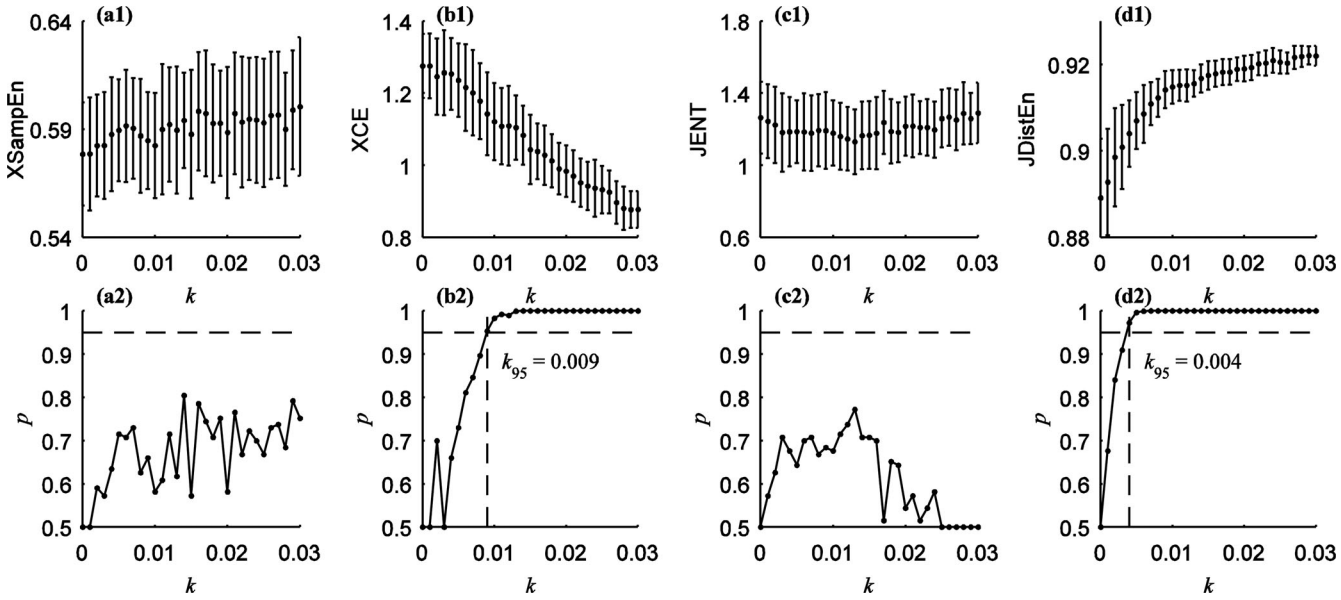

Fig. 1. Quantification of the sensitivity of four methods for the identical coupled Rössler system ($\nu = 0$). Panels in the upper row show the corresponding distributions of XSampEn (a1), XCE (b1), JENT (c1), and JDistEn (d1) represented with mean value $\pm$ one standard deviation. Lower panels show the $p_H\ (k)$ for XSampEn (a2), XCE (b2), JENT (c2), and JDistEn (d2), respectively. Horizontal dashed lines represent the sensitivity threshold value 0.95; vertical dashed lines in (b2) and (d2) represent the critical coupling strengths k_{95}.

$p_H\ (k)$ drops below the threshold value 0.95, but it may be able to represent a second crossing of this value. Then the k value for the second crossing was used as the critical coupling strength, e.g., k_{95} for JDistEn shown in Fig. S2(d2).

b) Coupling Estimation With 1000 Sampling Points: Fig. 2 and Fig. S3 (see the Online Supplement) show the estimation of coupling for $\nu = 0$ and $\nu = 0.02$, respectively. Examples of trajectories of observables are also shown in the upper panels of Figs. 2 and S3 by plotting the response observable versus the drive observable values for an intuitive expression on the coupled dynamics.

Fig. 2(b1) shows an increased XSampEn with the coupling strength k increased from zero to 0.1, indicating a failure of XSampEn since, by definition, it should decrease as k increase. As k continues to increase from 0.1 to 0.2, XSampEn begins to decrease. Next, as shown in Fig. S3(b1), for the almost identical coupled Rössler system with $\nu = 0.02$, XSampEn decreases with k from 0.03 to 0.06 after an initial increase from zero to around 0.03, which is followed by a plateau with k from 0.06 to 0.14. XSampEn then decreases again with $k = 0.14$ to 0.2. The results suggest that XSampEn performed well only for relatively strong coupling dynamics.

Figs. 2(b2) and S3(b2) both show an overall reduced XCE with the coupling strength k. But Fig. 2(b2) also shows a plateau from $k = 0.03$ to 0.13. An initial increasing phase is present for the almost identical coupled Rössler system with $\nu = 0.02$, as shown in Fig. S3(b2). The results suggest that XCE should be capable of detecting strong coupling for coupled Rössler system, whereas special attention should be paid when it is used for weak coupling analysis.

Fig. 2(b3) shows that JENT increases slightly with k for the identical coupled Rössler system with $\nu = 0$. However, when it is for the coupled system with $\nu = 0.02$, the results of JENT are totally unacceptable.

JDistEn increases with the coupling strength k for both coupled systems with $\nu = 0$ and $\nu = 0.02$, as shown in Fig. 2(b4) and Fig. S3(b4), respectively. Different from the other three methods, the increasing trends of JDistEn for weak coupling are extremely significant. However, the increase becomes very slight when $k > 0.05$ for the coupled Rössler system with $\nu = 0$. It even stops and remains unchanged when $k > 0.15$ for the coupled Rössler system with $\nu = 0.02$. The results confirm that JDistEn was superior for detecting weak coupling. However, the weak ability of JDistEn to differentiate between dynamics with strong coupling strengths was also indicated.

c) Coupling Estimation With 100 Sampling Points: The lower panels of Figs. 2 and S3 show the performance as the data length decreased to 100 points. The standard deviations of all four methods increased significantly, suggesting a common effect of insufficient data samples. Specifically, XSampEn resulted in invalid values for some realizations, and thus, no ensemble result was shown for a certain k values (see Fig. 2(c1) and Fig. S3(c1)]. XCE, as shown in Fig. 2(c2), showed a similar trend to the result in Fig. 2(b2). But when it is for the coupled system with $\nu = 0.02$, the results for XCE seemed to be a bit complicated: with an overall decreasing trend after an initial fluctuating phase from $k = 0$ to 0.07. JENT showed an overall slight increase trend for both coupled systems with $\nu = 0$ and $\nu = 0.02$, as shown in Fig. 2(c3) and Fig. S3(c3).

JDistEn behaved similarly to XCE. For the identical coupled Rössler system with $\nu = 0$, JDistEn shown similar to the 1000 points' case whereas for the coupled system with $\nu = 0.02$, there was a decreasing phase of JDistEn from $k = 0.03$ to 0.07. It was noted that both XCE and JDistEn indicated an inversely

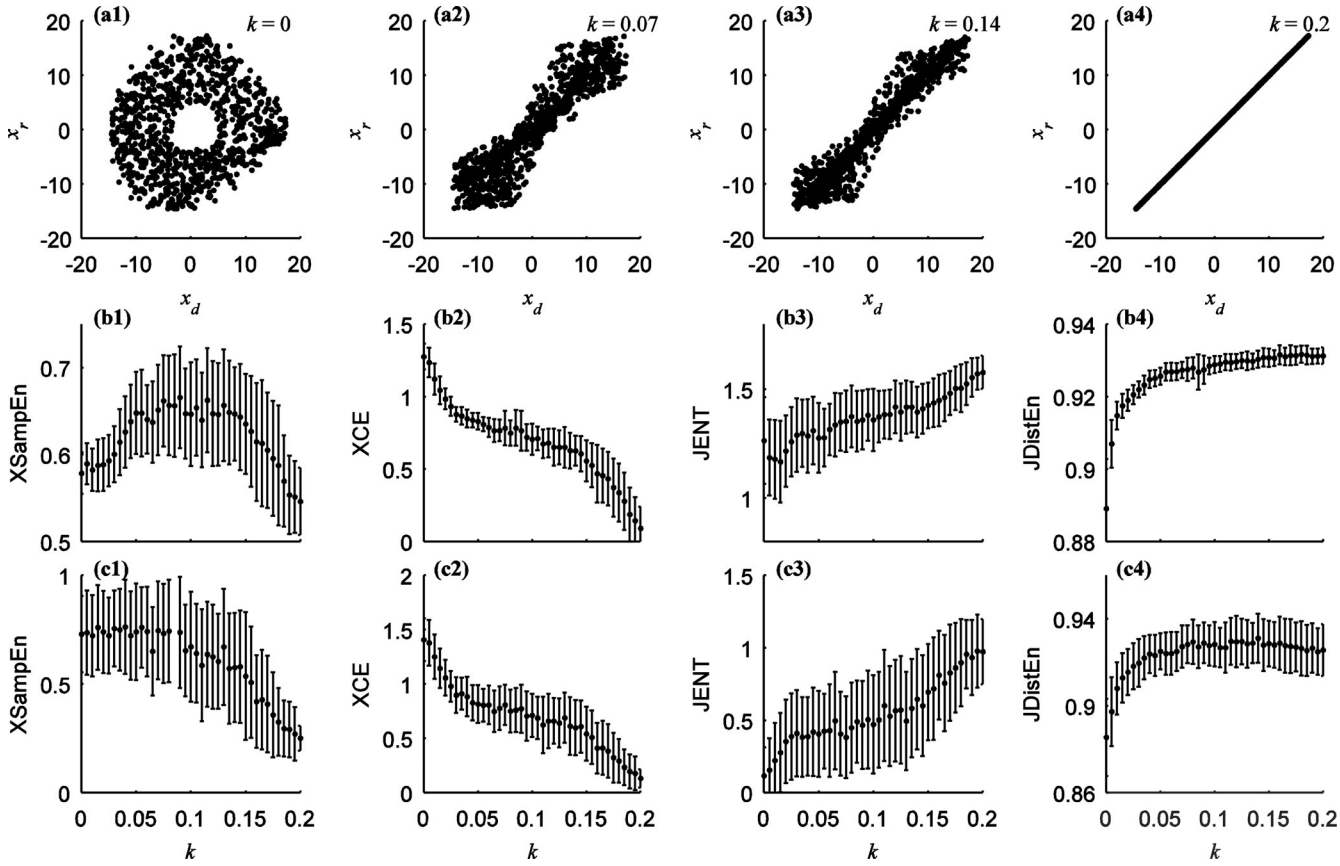

Fig. 2. Estimation of coupling for the identical coupled Rössler system ($\nu = 0$). Panels in the upper row show the plot of response observable versus drive observable values, with each coupling strength marked at the top-right corner. Middle panels show the results estimated by XSampEn (b1), XCE (b2), JENT (b3), and JDistEn (b4), respectively, with data length of 1000 points. Lower panels show the estimation results of the four methods, but with the data length used for the estimation decreased to just 100 points. Only partial results for XSampEn are shown in (c1), because invalid results were constantly produced for the other parts.

varying trend from $k = 0.03$ to 0.07. This could be linked with the standard deviations of both XCE and JDistEn with k values that were significantly larger than their neighboring values, as shown in Fig. S3(b2) and (b4) from the results using 1000 points. Thus, it may be worth exploring what happened in the dynamics of the almost identical coupled Rössler system with those k values. Nevertheless, the results again suggest that, for the coupled Rössler system, JDistEn was superior to the other three methods for detecting weak coupling.

B. Evaluation of Coupled NMM

1) Model Description: Although the coupled Rössler system was useful to test the performance of different methods in the theoretical domain, it does not provide any specific physiological meaning. We next employed the NMM developed from the mean activity of a whole neuronal population [32]. This model provides the possibility to understand general features of macroscopic brain signals, such as EEG in the field of neuroscience. NMM can model different EEG kinetics by simply tuning the state variables, and hence, can produce various waves, ranging from delta to gamma. David and Friston introduced a weight parameter to control the relative contributions of fast (e.g., gamma) and slow (e.g., alpha) populations in order to produce waves with dual kinetics. This scheme can be easily implemented to produce multiple kinetics to mimic real-world EEG data [33]. Nonlinear coupling is further generated by introducing the output of one "distant" area as part of the input while feeding the output of the current area back to the distant one [33]. Both outputs are scaled by a coupling parameter k prior to transmitting to other areas so as to simulate bivariate series with different coupling strengths. The details of the coupled dual-kinetics NMM and its simulation approach are provided in the Online Supplement.

2) Estimation of Coupling Strength: Similarly to our findings with coupled Rössler system, we observed variations in XSampEn, XCE, JENT, and JDistEn with k varied from zero (uncoupled dynamics) to 1 (completely coupled dynamics) in steps of 0.05. The embedding dimension m and time delay τ were determined by the differential entropy-based method [31], which suggested $m = 4$ and $\tau = 5$ for both channels (see Online Supplement). The threshold was $r = 0.15$ for XSampEn, quantization level $\xi = 6$ for XCE, and minimum diagonal line length $l_{\min} = 2$ for JENT.

3) Effect of Data Length: The coupling analysis in Section III-B-2 was reperformed on the dual-kinetics NMM with all observables restricted to the first 100 sampling points.

It should be noted here that the sensitivities of the four methods were quantified directly using the evaluation results in Sections III-B-2 and III-B-3. We did not perform weak coupling

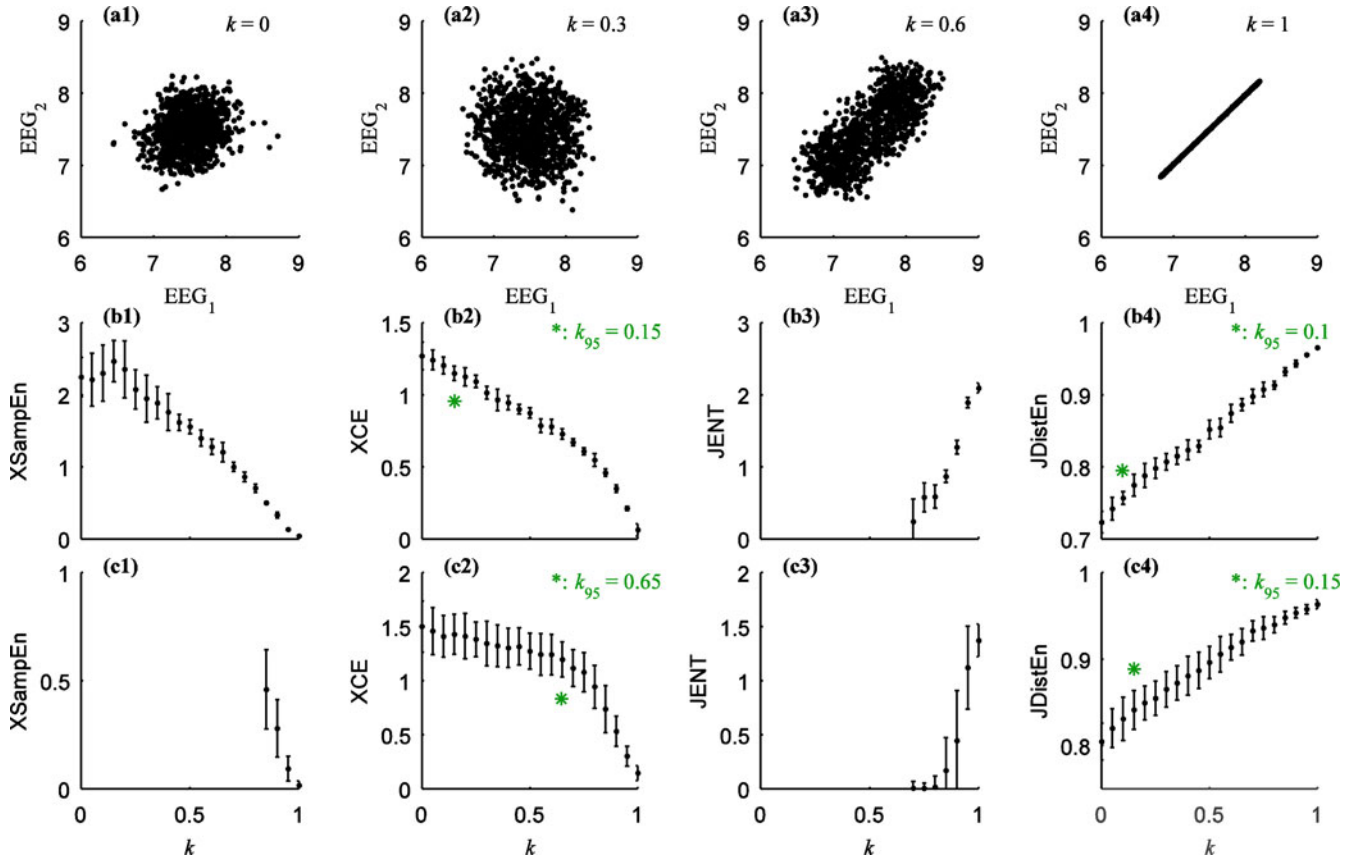

Fig. 3. Estimation of coupling for the coupled dual-kinetics NMM. Panels in the upper row show the plot of the second simulated EEG channel versus the first channel, with each coupling strength marked at the top-right corner. Middle panels show the results estimated by XSampEn (b1), XCE (b2), JENT (b3), and JDistEn (b4), respectively, with data length of 1000 points. Lower panels show the estimation results of the four methods, but with the data length used for the estimation restricted to 100 points. Only partial results for XSampEn and JENT are shown in (c1) and (c3), because invalid results were constantly produced for the other parts. Asterisks in (b2), (b4), (c2), and (c4) indicate the critical coupling strengths k_{95} with each specific value marked in the top-right corner.

simulation with fine steps as we did for the coupled Rössler system because the dynamics changed very weakly for a variation of 0.05 (simulation step we used for the coupled dual-kinetics NMM) in coupling strength, and another important reason was that the simulation of the coupled dual-kinetics NMM was time consuming.

4) Evaluation Results on the Coupled Dual-Kinetics NMM: Fig. 3 incorporates the results of the four methods with variations of k (middle panel). For a visual expression of the coupled dynamics, we also show the EEG from the second channel plotted versus the first in the upper panel of Fig. 3.

a) Coupling Estimation With 1000 Sampling Points: XSampEn and JENT both showed acceptable performance for only strong coupling dynamics, as shown in Fig. 3(b1) to (b3). For weak coupling cases, XSampEn showed great fluctuations among different realizations and the average level decreased with the coupling strength k after an initial increase stage, which was very similar to its behavior for both coupled Rössler systems. JENT only showed sensitive to strong coupling since it appeared invalid for all $k \leq 0.7$. XCE showed a negative relation to k, but the relationship appeared nonlinear since it decreased faster for strong coupling. For weak coupling dynamics, XCE seemed to have poor discrimination between different coupling strengths. By comparison, the proposed JDistEn showed a linearly positive relation to k with good discrimination for not only strong coupling dynamics but also weak coupling cases. The sensitivity analysis further confirmed this improvement, which suggested a critical value $k_{95} = 0.15$ for XCE and an improved critical value $k_{95} = 0.1$ for JDistEn. This phenomenon also supports our sensitivity analysis described in Section *A*, showing that XCE generally performs well for strong coupling dynamics but is not suitable for detecting weak coupling.

b) Coupling Estimation With 100 Sampling Points: Coupling performance from the four methods with a data length of 100 points is shown in the lower panel of Fig. 3. XSampEn and JENT only showed sensitive to strong coupling dynamics. They both yielded invalid results for weak coupling cases. Although XCE showed acceptable performance with $k \geq 0.7$, its distinguishability for weak coupling was worsened by the lack of data samples, as shown in Fig. 3(c2), which suggests a critical coupling strength $k_{95} = 0.65$. Our proposed JDistEn showed good performance for all coupling strengths with only a small increase in the critical value (from 0.1 for the 1000 points' case to 0.15), as shown in Fig. 3(c4).

It can therefore be concluded from these simulation studies that the three traditional methods—XSampEn, XCE, and

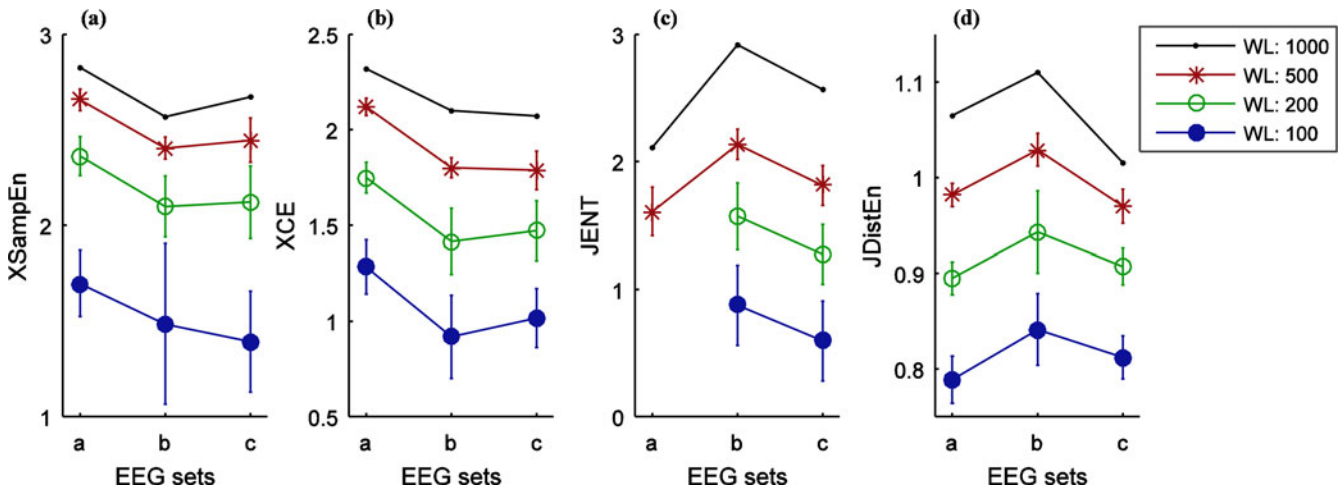

Fig. 4. Estimation of coupling for the rat EEG data with different analyzing window lengths. WL = window length.

JENT—generally perform well for strong coupling dynamics but are usually not suitable for detecting weak coupling. JDistEn showed comparable performance for strong coupling dynamics. More promisingly, it showed significant improvement in sensitivity for detecting weak coupling. This superiority is obvious even with short series. However, the coupling direction has not been considered in our simulation. The current algorithm for JDistEn may not be able to reflect the coupling direction, which should be a potential limitation (among the four, only XCE can [16]).

It should be noted that in using all four methods, we did not obtain zero values for uncoupled dynamics ($k = 0$). This is quite different from the methods for generalized synchronization [8] or phase synchronization [11] and traditional linear methods such as crosscorrelation. The nonzero values resulted from the complex structural information that still exists in the state space of uncoupled dynamics. In addition, those values are not necessarily the same for different uncoupled dynamics (simply because the structures of their state spaces are different from each other); hence, their changes relative to the uncoupled dynamics are in fact of more value than their absolute levels. Anyway, this problem may indicate an undesirable specificity of those methods. The use of surrogate data analysis could allow the investigation of the specificity [12]. Another applicable way could be to derive a special coupling measure based on JDistEn as has done for XCE (where a derived coupling measure was defined as the conditional entropy of target series subtracted by XCE) [16].

IV. Evaluation of Experimental Data

A. Coupling Analysis Between Bivariate Rat EEG Data

Abnormal spike discharges in EEG have been recognized as a prominent feature of incipient epileptic seizures, and these discharges are usually coupled among cortical areas [34]. It is thus of great clinical significance to estimate coupling from EEG data. In this section, we describe how our proposed JDistEn was tested on a publicly available rat EEG database which includes both normal EEG data and data containing spike discharges [35].

1) Rat EEG Database: The database is composed of five pairs of EEG recordings from electrodes placed on the left and right frontal cortex of male adult WAG/Rij rats (a genetic animal model of human epilepsy). Signals have already been filtered between 1∼100 Hz and digitized at 200 Hz [34, 36]. Among the five recordings, set a is from a normal case, and sets b to e are from four cases with spike discharges. The first three cases were used and investigated in this study since there is *a priori* information regarding their coupling levels according to several published investigations [23], [34], [36]. Set b is the most synchronized with the highest coupling between channels. Set a has been shown to have an overall higher coupling strength than set c, as suggested by both linear and nonlinear methods [34]. It is expected that a good method should be able to detect their coupling differences. Furthermore, set b shows a transition from ictal (with spike discharges) to interictal (no spike) periods at the final stage of the recording, which is also expected to be detected.

2) Estimation of Coupling Strength: The four methods (XSampEn, XCE, JENT, and JDistEn) were applied directly to the three pairs of EEG recordings. Additionally, although there is *a priori* information on the overall coupling strengths among the three datasets, there is currently no information on their coupling status given a specific time window. To elucidate the concerns rigorously, we also performed coupling analysis on sections with different lengths. Specifically, the measures were performed on each of the three pairs of EEG recordings using a moving time window of 500, 200, and 100 points, respectively, with 99% overlap between subsequent windows.

The m and τ were set at 2 and 4, respectively, according to the differential entropy-based method [31] (see Online Supplement for more information). The threshold r was set at 0.25 (a larger r can, to some extent, avoid the presence of invalid $\ln 0$ when the data length was relatively small) for XSampEn, ξ at 6 for XCE, and $l_{\min}$ at 2 for JENT.

3) Evaluation Results for Rat EEG Data: Fig. 4 incorporates the performance of the four methods on rat EEG data with different analyzing window lengths. Among the four methods, only JDistEn correctly ranked their overall coupling differences

[34]. According to the study by Quian Quiroga *et al*. [34], the weak coupling in set c may be caused by the large time lag between spikes. In addition, because of the random appearance of set a, it is also difficult to estimate the level of coupling solely by visual inspection. However, we can observe some patterns within specific time windows appearing simultaneously between channels in both sets.

The results confirmed the above concern, as suggested in Fig. 4. Despite the fact that XSampEn and XCE still indicated highest coupling in set a, they both failed to differentiate between sets b and c as the window length decreased to 500 points or less. JENT performed better as compared with XSampEn and XCE since it could still make a clear distinction among the three datasets as the window length decreased to 500 points. But it constantly resulted in invalid results for set a with shorter window lengths (200 and 100), although it could still tell the difference between sets b and c. JDistEn performed best since it could separate the three datasets out for all lengths of analyzing windows. However, despite the fact that highest coupling in set b was indicated for all window lengths, the estimated coupling strengths in set a and set c were not in the same order—for window length equaling 1000 (whole recording) and 500, JDistEn suggested that set a had higher coupling than set c, whereas for window lengths of 200 and 100 points, the coupling in set c was stronger. This stronger average coupling in set c may be introduced by the synchronized spike-like patterns within some time windows. Thus, JDistEn analysis for extremely short EEG data has potential, since we can expect that transient synchronized spike discharges very likely cannot be detected by longtime analysis.

An accurate detection of a transition from interictal to ictal may help physicians notice an incipient epileptic attack. JDistEn can potentially play an important role in such an application. Set b showed a perfect reverse transition from interictal to ictal period at its final stage, as shown in Fig. 5. JDistEn could accurately detect this transition indicated by a clear decrease. Note that JENT also showed a decreased value within this transition phase. Its main disadvantage is that it constantly resulted in invalid values for set a.

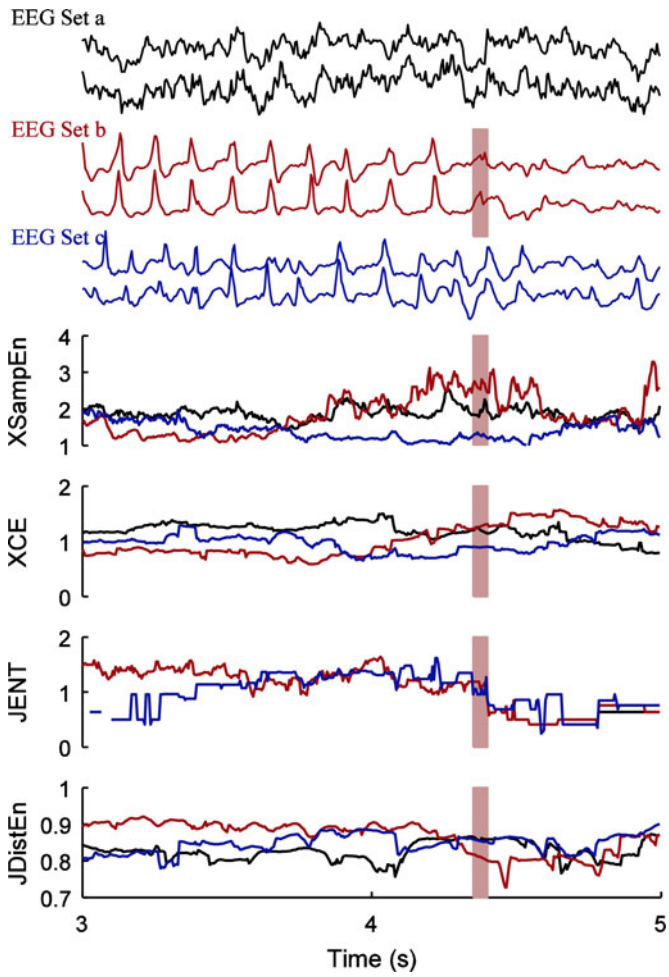

Fig. 5. EEG signals (sets a, b, and c, shown only episodes from 3 to 5 s each) from right and left cortical intracranial electrodes (upper panel) and the time evolution of XSampEn, XCE, JENT, and JDistEn (calculated every 100 points) for each set (lower four panels). EEG data channels are plotted with offsets for better visualization. Vertical bars indicate a transition in set b from ictal to interictal phase.

B. Coupling Analysis Between RRI and DTI Data

The RRI extracted from electrocardiograms (ECGs) has been widely applied to investigate cardiovascular autonomic regulation [37]. An RRI is physiologically composed of two complementary mechanical intervals which indicate separately the duration of the cardiac systolic and diastolic phases. As a result, the RRI can be decomposed into a systolic time interval series (STI) and a DTI. In addition, the beat-to-beat fluctuation in RRI is preferentially expressed in DTI, since the STI remains relatively stable to support periphery tissues steady-going blood supplies. In addition to the RRI analysis, the coupling between RRI and DTI has been reported in healthy elderly subjects [38], heart failure (HF) patients [39], and patients with diabetic autonomic neuropathy [40]. In this study, the RRI-DTI coupling in HF patients in comparison with healthy volunteers was examined to investigate the suitability of JDistEn in such applications.

1) RRI and DTI Data: The RRI and DTI data in this study were derived from simultaneously recorded ECG and radial artery pressure pulse signals (5-min long) measured by a Cardiovascular Function Detection Device (CV FD-I, Jinan Huiyironggong Co., Ltd, China). This study received a full ethical approval from the Qilu Hospital of Shandong University. Thirty-four HF patients and 33 healthy volunteers were recruited, matched by age and gender. Table I shows their basic clinical characteristics. Detailed clinical information with the measurement protocol and signal preprocessing approaches can be found in our previous publication [28].

Briefly, the R waves of the ECG signal, as well as the systolic feet and dicrotic notches of arterial pulse signals, were detected by customized MATLAB software. The DTI was constructed from the interval between the dicrotic notch and the systolic foot in the subsequent cycle. Anomalous intervals arising from ectopic beats or poor signal quality were filtered out prior to the following coupling analyses [28], [38], [39]. Fig. 6 shows an example of the construction of RRIs and DTIs from a healthy volunteer and an HF patient.

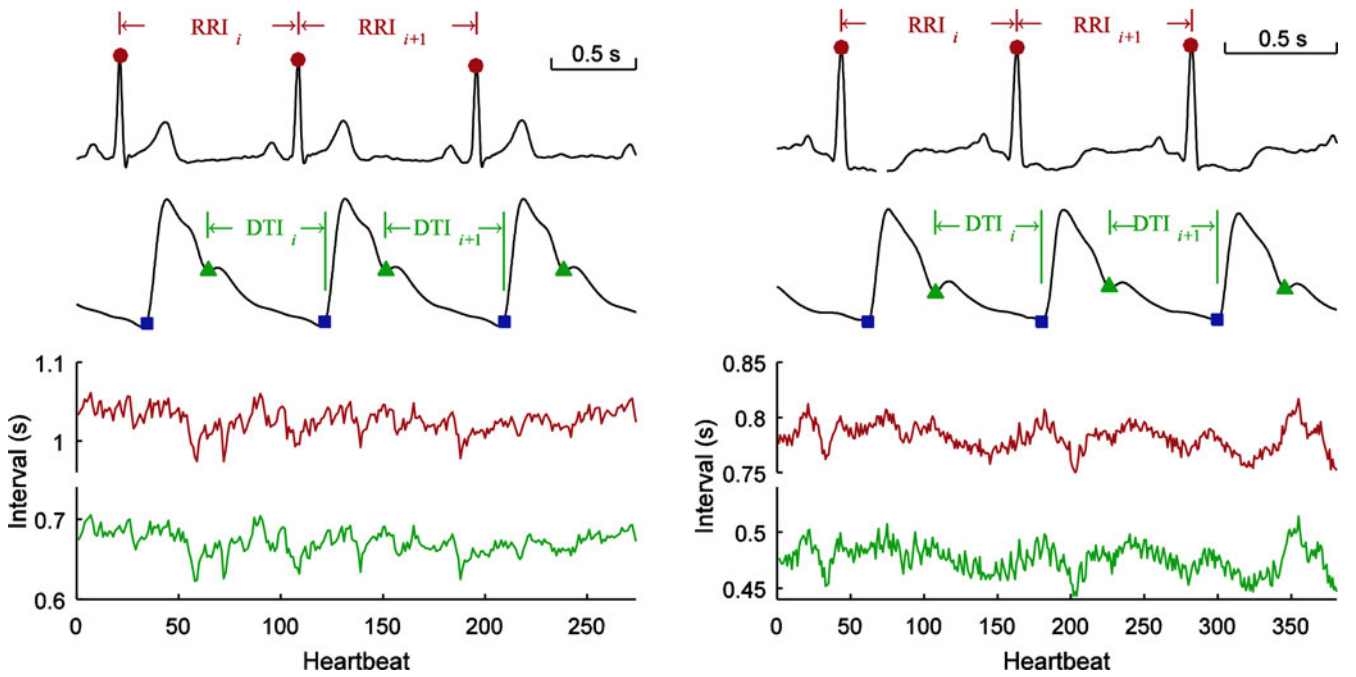

Fig. 6. Construction of RRIs and DTIs from ECGs and RAP signals (top panel). The 5 min RRI and DTI series are shown in the bottom panel. Left panel is from a healthy volunteer (age: 65, sex: male) and right panel from a HF patient (age: 68, sex: male).

TABLE I
PHYSIOLOGICAL CHARACTERISTICS FOR HEALTHY VOLUNTEERS AND HF PATIENTS

Variables	Healthy volunteers	HF patients	p value
No.	33	34	–
Men	18	21	0.55
Age (years)	56 ± 8	59 ± 9	0.29
BMI (kg/m^2)	24 ± 3	25 ± 4	0.16
SBP (mmHg)	114 ± 13	118 ± 14	0.23
DBP (mmHg)	72 ± 9	75 ± 9	0.18
LVEF (%)	65 ± 4	39 ± 7	<0.01

Data are expressed as number or mean $\pm$ standard deviation. No. = number, BMI = body mass index, SBP = systolic blood pressure, DBP = diastolic blood pressure, LVEF = left ventricular ejection fraction.

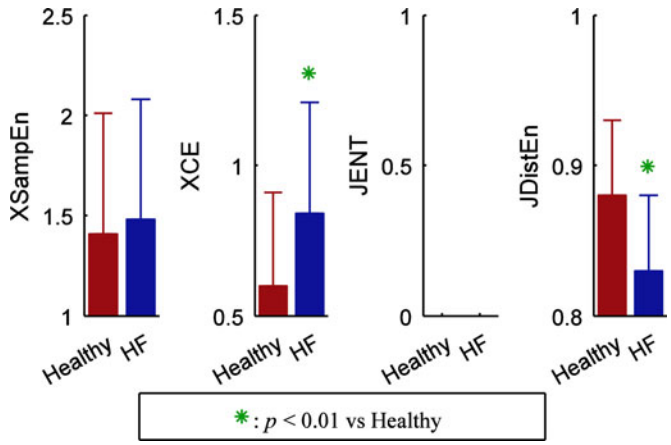

Fig. 7. Estimation of coupling between RRI and DTI data for healthy volunteers and HF patients. Shown are ensemble results for each method in terms of median value plus interquartile range. JENT constantly resulted in invalid values; thus no ensemble result is shown.

2) RRI-DTI Coupling Analysis: The proposed JDistEn and the traditional XSampEn, XCE, and JENT methods were all performed for the RRI-DTI series. The input parameters m and τ were set at 2 and 3, respectively, for both the RRI and DTI series (see Online Supplement). The threshold value r was set at 0.25 for XSampEn, quantization level ξ at 6 for XCE, and diagonal length $l_{\min}$ at 2 for JENT. Statistical analysis was performed to compare the coupling difference between the two groups using the Mann–Whitney U test. Statistical significance was accepted at $p < 0.05$. All statistical analyses were performed using SPSS software (Ver. 20.0, IBM, Armonk, NY, USA).

3) Results for RRI-DTI Coupling Analysis: As shown in Fig. 6, for both the healthy subject and HF patient, RRI and DTI time series changed in a similar pattern, indicating strong coupling dynamics. Their coupling difference is therefore difficult to detect visually. By employing our proposed JDistEn and the other three methods, as shown in Fig. 7, XSampEn could not distinguish between the two groups, indicating its poor performance for short data. JENT consistently resulted in invalid values for both groups (over 30% for healthy subjects and 75% for HF patients). The appearance of those invalid results may be due to the lack of diagonal lines introduced by both the short data length and the thresholding procedure. Both XCE and our proposed JDistEn showed statistically significant change, which supports the finding from our simulation studies that JDistEn yields a comparable performance for detecting strong coupling. In addition, the significantly increased XCE and decreased JDistEn in HF patients both suggested a loss of

RRI-DTI coupling with HF, which would be applicable for the noninvasive evaluation of cardiovascular autonomic control.

V. Discussion

A. Further Explanation of JDistEn

We have previously reported the performance of DistEn on a short univariate dataset [28]. The ePDF estimation from all the intervector distances, which is a global quantification approach, is thought to account for this improvement. The JDistEn algorithm proposed in this study inherited this advantage; therefore, a good performance for small bivariate datasets is expected. The evaluations in this study using simulation models and experimental data have supported this assumption.

The use of the distribution of all intervector distances is one noticeable advantage of DistEn and JDistEn. However, there is another published study employed similar type of estimation based on delay vectors [41]. This so-developed "delay vector variance (DVV)" algorithm spans the distribution of pairwise distances between not only delay vectors but also the targets of delay vectors (the following sample of a certain delay vector) in order to examine the local predictability. The algorithm has proved to be capable of robustly detecting determinism and nonlinearity in time series using both synthetic and real-world standard signals [41]. A further comparison between our method and DVV should be of significance which, however, has scheduled in our future worklists.

Another crucial aspect of JDistEn is the construction of the distance matrix from both data channels. The approach in (4) was used to construct a joint distance matrix through the complementary set of the geometric mean of all complementary sets of the (univariate) distance matrices from different data channels. Under a microscopic perspective, JDistEn is screened by the difference among the distances of the corresponding pairs of vectors from different data channels (see Fig. S4 for a geometric explanation of the idea behind the joint distance matrix). The joint distance matrix will be equal to any univariate matrix when all data channels are completely coupled. In this case, JDistEn will be the same as DistEn for any data channel. Therefore, coupling analysis from JDistEn is not an absolute estimate. Result of JDistEn relates to the complexity of all data channels or the intrinsic property of the system being analyzed. Comparison of JDistEn results for different dynamics should be of meaningless. We have illustrated this concern in our simulation studies. However, the correspondence between coupling degree and complexity could be a potential limitation since in particular cases perfectly coupled dynamics may alter their intrinsic complexity. The three comparison algorithms have the same property—their relative changes provide much more meaningful information than their absolute values.

In addition, the joint distance matrix is initially defined for a bivariate case. The extension to a multivariate case will be very straightforward by redefining (4) in a multiple channel way, that is,

$$\mathbf{JD} = \mathbf{J} - \sqrt[\psi]{\prod (\mathbf{J} - \mathbf{D}_{\varphi})} \tag{11}$$

where again, $\mathbf{J}$ indicates the all-ones matrix and $\mathbf{D}_{\varphi}$ the distance matrix of channel φ ($\varphi = 1, 2, \ldots, \psi$). The performance of this multivariate extension form of JDistEn for analyzing multichannel data will thus deserve further elucidation. One potential comparison algorithm will be multivariate sample entropy [18, 19].

It may also be acceptable to directly apply the geometric mean of all univariate distance matrices (i.e., $\mathbf{JD} = \sqrt[\psi]{\prod \mathbf{D}_{\varphi}}$). However, this version of joint distance matrix may introduce bias when zero occurs. For example, one distance is 0.9 and the corresponding one from another channel is zero; the geometric mean will be zero, which mistakenly treats them as belonging to the same neighbor. However, using the joint distance of 0.68 ($1 - \sqrt{(1-0) \times (1-0.9)} \approx 0.68$), a rational correction is provided to the bias.

Furthermore, $\mathbf{JD}$ can be converted to the joint recurrence plots by thresholding each $\mathbf{D}_{\varphi}$ first in (4) by the threshold parameter *r* [20]. It has been noticed, in some previous studies on the quantification of joint recurrence plots, that the distance matrix was introduced and named as an unthresholded recurrence plot, a global recurrence plot, or similarly as a distance plot [17]. However, to the best of our knowledge, it is most often applied as a qualitative tool rather than a quantitative method.

B. Application Perspective

We demonstrated good performance of JDistEn on bivariate rat EEG data. The results agreed with our simulation study that the traditional methods, including XSampEn, XCE, and JENT, failed to track the weak coupling changes when small datasets were used. The traditional coupling methods may be capable when a sufficiently large dataset is available. However, such methods of *post hoc* analysis after collecting "enough" data are less practical in a real clinical setting. For example, physicians should be warned by a change in these coupling measures that a patient being monitored may have an epileptic attack. With JDistEn, it is possible to be noticed by the physicians almost immediately after the epileptic seizure (e.g., in Fig. 5, a 0.5 s time window can support a sensitive detection). Our results also showed that screening the JDistEn profiles may reveal the evolution of coupling with time. With this information, the prediction of future events is possible. This is also one of the reasons that this study focused on the short-term application.

Furthermore, JDistEn was applied to evaluate short-term RRI-DTI coupling. RRI analysis has been accepted as a useful tool for assessing the cardiovascular control mechanism. However, how to robustly estimate the RRI features within a short screening time remains a significant challenge, partly because the linear time- or frequency-domain approaches are limited by the nonstationary nature of the RRI series, and the traditional nonlinear measures require a sufficiently large dataset. This defect limits the application of using short-term RRI and DTI in various biomedical applications where long-term data collecting cannot be done. The validation results on human clinical data showed a significantly reduced JDistEn of RRI-DTI in HF patients, suggesting JDistEn very promising for examining short-term cardiovascular control mechanism in clinical practice.

VI. Conclusion

A novel JDistEn method was developed in this study for the detection of coupling in short physiological series. Both simulation and experimental studies proved that JDistEn has remarkably higher sensitivity for detecting weak coupling especially for short series. This study suggests that our proposed JDistEn should be promising for continuous and even real-time monitoring of coupling in physiological signals in clinical practice.

Acknowledgment

P. Li thanks Dr. Norbert Marwan from the Potsdam Institute for Climate Impact Research, Potsdam, Germany, for providing access to the crp toolbox [42]. The authors would like to thanks the anonymous reviewers for their constructive comments that greatly contributed to improving the quality of our paper.

References

[1] L. Faes *et al.*, "Information dynamics of brain–heart physiological networks during sleep," *New J. Phys.*, vol. 16, no. 10, pp. 105005-1–105005-20, 2014.
[2] R. P. Bartsch *et al.*, "Phase transitions in physiologic coupling," in *Proc. Nat. Acad. Sci. USA.*, vol. 109, no. 26, pp. 10181–10186, 2012.
[3] J. Lee *et al.*, "Transfer entropy estimation and directional coupling change detection in biomedical time series," *Biomed. Eng. Online*, vol. 11, no. 1, pp. 19-1–19-17, 2012.
[4] P. Lowdon *et al.*, "Heart rate and blood pressure interactions during attempts to consciously raise or lower heart rate and blood pressure in normotensive subjects," *Physiol. Meas.*, vol. 32, no. 3, pp. 359–367, 2011.
[5] L. Faes *et al.*, "Information domain approach to the investigation of cardiovascular, cardio-pulmonary, and vasculo-pulmonary causal couplings," *Front. Physiol.*, vol. 2, pp. 80-1–80-13, 2011.
[6] J. Dauwels *et al.*, "A comparative study of synchrony measures for the early diagnosis of Alzheimer's disease based on EEG," *NeuroImage*, vol. 49, no. 1, pp. 668–693, 2010.
[7] L. Faes *et al.*, "Measuring connectivity in linear multivariate processes: Definitions, interpretation, and practical analysis," *Comput. Math. Methods Med.*, vol. 2012, no. 140513, pp. 140513-1–140513-18, 2012.
[8] N. F. Rulkov *et al.*, "Generalized synchronization of chaos in directionally coupled chaotic systems," *Phys. Rev. E*, vol. 51, no. 2, pp. 980–994, 1995.
[9] S. J. Schiff *et al.*, "Detecting dynamical interdependence and generalized synchrony through mutual prediction in a neural ensemble," *Phys. Rev. E*, vol. 54, no. 6, pp. 6708–6724, 1996.
[10] M. G. Rosenblum *et al.*, "Identification of coupling direction: application to cardiorespiratory interaction," *Phys. Rev. E*, vol. 65, no. 4 Pt 1, pp. 041909-1–041909-11, 2002.
[11] M. G. Rosenblum *et al.*, "Phase synchronization of chaotic oscillators," *Phys. Rev. Lett.*, vol. 76, no. 11, pp. 1804–1807, 1996.
[12] D. A. Smirnov and R. G. Andrzejak, "Detection of weak directional coupling: Phase-dynamics approach versus state-space approach," *Phys. Rev. E*, vol. 71, no. 3 Pt 2A, pp. 036207-1–036207-13, 2005.
[13] K. S. Nikita *et al.*, "Editorial: Special issue on mobile and wireless technologies for healthcare delivery," *IEEE Trans. Biomed. Eng.*, vol. 59, no. 11, pp. 3083–3089, Nov. 2012.
[14] S. M. Pincus *et al.*, "Older males secrete luteinizing hormone and testosterone more irregularly, and jointly more asynchronously, than younger males," *Proc. Nat. Acad. Sci. USA.*, vol. 93, no. 24, pp. 14100–14105, 1996.
[15] T. Zhang *et al.*, "Cross-sample entropy statistic as a measure of complexity and regularity of renal sympathetic nerve activity in the rat," *Exp. Physiol.*, vol. 92, no. 4, pp. 659–669, 2007.
[16] A. Porta *et al.*, "Conditional entropy approach for the evaluation of the coupling strength," *Biol. Cybern.*, vol. 81, no. 2, pp. 119–129, 1999.
[17] N. Marwan *et al.*, "Recurrence plots for the analysis of complex systems," *Rhys. Rep.*, vol. 438, nos. 5/6, pp. 237–329, 2007.
[18] M. U. Ahmed and D. P. Mandic, "Multivariate multiscale entropy analysis," *IEEE Signal Process. Lett.*, vol. 19, no. 2, pp. 91–94, Feb. 2012.
[19] M. U. Ahmed and D. P. Mandic, "Multivariate multiscale entropy: A tool for complexity analysis of multichannel data," *Phys. Rev. E*, vol. 84, no. 6 Pt 1, pp. 061918-1–061918-10, 2011.
[20] M. C. Romano *et al.*, "Multivariate recurrence plots," *Phys. Lett. A*, vol. 330, nos. 3/4, pp. 214–223, 2004.
[21] N. Marwan, "How to avoid potential pitfalls in recurrence plot based data analysis," *Int. J. Bifurcation Chaos*, vol. 21, no. 4, pp. 1003–1017, 2011.
[22] P. Li *et al.*, "Testing pattern synchronization in coupled systems through different entropy-based measures," *Med. Biol. Eng. Comput.*, vol. 51, no. 5, pp. 581–591, 2013.
[23] H. Xie *et al.*, "A comparative study of pattern synchronization detection between neural signals using different cross-entropy measures," *Biol. Cybern.*, vol. 102, no. 2, pp. 123–135, 2010.
[24] S. M. Pincus, "Approximate entropy as a measure of system complexity," in *Proc. Nat. Acad. Sci. USA.*, vol. 88, no. 6, pp. 2297–2301, 1991.
[25] J. S. Richman and J. R. Moorman, "Physiological time-series analysis using approximate entropy and sample entropy," *Amer. J. Physiol. Heart Circ. Physiol.*, vol. 278, no. 6, pp. H2039–H2049, 2000.
[26] A. Porta *et al.*, "Entropy, entropy rate, and pattern classification as tools to typify complexity in short heart period variability series," *IEEE Trans. Biomed. Eng.*, vol. 48, no. 11, pp. 1282–1291, Nov. 2001.
[27] C. L. Webber Jr and J. P. Zbilut, "Recurrence quantification analysis of nonlinear dynamical systems," in *Tutorials in Contemporary Nonlinear Methods for the Behavioral Sciences*, M. A. Riley and G. V. Orden, Eds. Arlington, VI, USA: Nat. Sci. Found., 2005, pp. 26–94.
[28] P. Li *et al.*, "Assessing the complexity of short-term heartbeat interval series by distribution entropy," *Med. Biol. Eng. Comput.*, vol. 53, no. 1, pp. 77–87, 2015.
[29] D. P. Doane, "Aesthetic frequency classifications," *Amer. Statist.*, vol. 30, no. 4, pp. 181–183, 1976.
[30] Z. Zheng and G. Hu, "Generalized synchronization versus phase synchronization," *Phys. Rev. E*, vol. 62, no. 6, pp. 7882–7885, 2000.
[31] T. Gautama *et al.*, "A differential entropy based method for determining the optimal embedding parameters of a signal," in *Proc. IEEE Int. Conf. Acoust., Speech, Signal Process.*, 2003, vol. 6, pp. 29–32.
[32] B. Jansen and V. Rit, "Electroencephalogram and visual evoked potential generation in a mathematical model of coupled cortical columns," *Biol. Cybern.*, vol. 73, no. 4, pp. 357–366, 1995.
[33] O. David and K. J. Friston, "A neural mass model for MEG/EEG: coupling and neuronal dynamics," *NeuroImage*, vol. 20, no. 3, pp. 1743–1755, 2003.
[34] R. Quian Quiroga *et al.*, "Performance of different synchronization measures in real data: A case study on electroencephalographic signals," *Phys. Rev. E*, vol. 65, no. 4, pp. 041903-1–041903-14, 2002.
[35] R. Quian Quiroga. EEG, ERP and single cell recordings database. [Online]. Available: http://www.vis.caltech.edu/∼rodri/data.htm
[36] R. Quian Quiroga *et al.*, "Event synchronization: A simple and fast method to measure synchronicity and time delay patterns," *Phys. Rev. E*, vol. 66, no. 4, pp. 041904-1–041904-9, 2002.
[37] G. Ernst, "The autonomic nervous system," in *Heart Rate Variability*, G. Ernst, Ed. London, U.K.: Springer-Verlag, 2014. pp. 27–49.
[38] P. Li *et al.*, "Age related changes in variability of short-term heart rate and diastolic period," in *Proc. Comput. Cardiol. Conf.*, 2013, pp. 995–998.
[39] P. Li *et al.*, "Coupling between short-term heart rate and diastolic period is reduced in heart failure patients as indicated by multivariate entropy analysis," *Comput. Cardiol.*, vol. 41, no. 7042988, pp. 97–100, 2014.
[40] M. H. Imam *et al.*, "Analysing cardiac autonomic neuropathy in diabetes using electrocardiogram derived systolic-diastolic interval interactions," *Comput. Cardiol.*, vol. 41, 7042985, pp. 85–88, 2014.
[41] T. Gautama *et al.*, "The delay vector variance method for detecting determinism and nonlinearity in time series," *Physica D*, vol. 190, nos. 3/4, pp. 167–176, 2004.
[42] N. Marwan. Cross recurrence plots toolbox. [Online]. Available: http://tocsy.pik-potsdam.de/CRPtoolbox/install.php

Peng Li (M'15) was born in Weishan, Shandong Province, China, in 1988. He received the B.S. and the Ph.D. degrees in biomedical engineering from Shandong University, Jinan, China, in 2009 and 2014, respectively.

He is currently a Postdoctoral Research Fellow with the School of Control Science and Engineering, Shandong University. His research interests include nonlinear analysis of cardiovascular dynamics, novel time-series analysis methods from nonlinear dynamics and statistical physics, and novel noninvasive techniques for evaluating the cardiovascular function.

Ke Li (M'15) received the B.S. degree in information engineering from Zhejiang University, Hangzhou, China, the M.S. degree in biomedical engineering from Shandong University, Jinan, China, and the Ph.D. degree in biomedical engineering from University of Technology of Troyes, Troyes, France, in 2003, 2006, and 2010, respectively.

He was a Research Assistant with the Institute of Myology in the Pitié-Salpétrière Hospital, Paris, France, in 2009, and a Postdoctoral Research Fellow with the Cleveland Clinic, Cleveland, OH, USA, from 2011 to 2013. He is currently an Associate Professor with the School of Control Science and Engineering, Shandong University. His research interest includes nonlinear dynamics of musculoskeletal and cardiovascular systems.

Chengyu Liu (M'14) received the B.Eng. and the Ph.D. degrees in biomedical engineering from Shandong University, Jinan, China, in 2005 and 2010, respectively.

From December 2010 to May 2013, he was a Postdoctoral Researcher at Shandong University, Jinan, China. From May 2013 to Novembor 2014, he was a Research Associate at Newcastle University, Newcastle upon Tyne, U.K. He is currently an Associate Professor with the Department of Biomedical Engineering, Shandong University. His research interests include physiological signal processing, including analytic methods for electrocardiography, pulse, and blood pressure signals, and entropy methods.

Dingchang Zheng received the B.Eng. degree in biomedical engineering from Zhejiang University, Hangzhou, China, in 2002, and the Ph.D. degree in medical physics from Newcastle University, Newcastle upon Tyne, U.K., in 2006.

He is currently the M.Sc. Program Leader in Medical Technology at Anglia Ruskin University, Cambridge, U.K. He was the Head of the Cardiovascular Physics & Engineering Research Group and a Senior Research Fellow at the Institute of Cellular Medicine, Newcastle University, Newcastle upon Tyne, U.K. He has a particular interest in new methods of physiological measurements and signal processing, and in understanding the electrical and mechanical principles of the heart and their relationships to the peripheral circulation.

Dr. Zheng is the winner of the Martin Black Annual Prize as coauthor of the best article published in the journal *Physiological Measurement* in 2011. He is also the winner of the 2009 JA Lodge Award from the Institution of Engineering and Technology (IET) for "Recognizing and Promoting Outstanding Work in the Field of Research and Development in Medical Engineering."

Zong-Ming Li (M'15-SM'15) received the B.Sc. degree in engineering mechanics from Southwest Jiaotong University in 1989, and the M.Sc. degree in engineering mechanics from the Chengdu University of Science and Technology (1992), both in Chengdu, Sichuan, China. He received the Ph.D. degree in kinesiology/biomechanics in 1998 from Pennsylvania State University, State College, PA, USA.

He is currently Associate Staff in the Department of Biomedical Engineering with joint appointments in the Departments of Orthopaedic Surgery and Physical Medicine & Rehabilitation, Cleveland Clinic, Cleveland, OH, USA. He has been a President of the World Association for Chinese Biomedical Engineers (2013–2015) and is a Fellow of American Institute for Medical and Biological Engineering. His research interest include biomechanics and motor control of the hand and wrist.

Changchun Liu received the B.S. and M.S. degree in automation from Shandong Industrial University (now merged into Shandong University), Jinan, China, in 1982 and 1987, respectively.

From 1993 to 2000, he was an Associate Professor in automation with the Department of Automation, Shandong University. Since 2000, he has been a Professor in Biomedical Engineering with the School of Control Science and Engineering, Shandong University. He headed the Research Group of Noninvasive Evaluation of Cardiovascular Function in Shandong University. He is the author of more than 100 articles, and he also holds more than 10 Chinese invention patents. His research interests include biomedical signal and image processing, biomedical measurements and devices, and physiological system modeling.

Prof. Liu received the first prize of the Science and Technology Award in technical invention awarded by the Ministry of Education, China, in 2003.